Modeling of Radiative Heat Transfer in 2D Complex Heat Recuperator of Biomass Pyrolysis Furnace: A Study of Baffles Shadow and Soot Volume Fraction Effects

Mohamed Ammar Abbassi, Kamel Guedri, Mohamed Naceur Borjini, Kamel Halouani, Belkacem Zeghmati

Abstract—The radiative heat transfer problem is investigated numerically for 2D complex geometry biomass pyrolysis reactor composed of two pyrolysis chambers and a heat recuperator. The fumes are a mixture of carbon dioxide and water vapor charged with absorbing and scattering particles and soot. In order to increase gases residence time and heat transfer, the heat recuperator is provided with many inclined, vertical, horizontal, diffuse and grey baffles of finite thickness and has a complex geometry. The Finite Volume Method (FVM) is applied to study radiative heat transfer. The blocked-off region procedure is used to treat the geometrical irregularities. Eight cases are considered in order to demonstrate the effect of adding baffles on the walls of the heat recuperator and on the walls of the pyrolysis rooms then choose the best case giving the maximum heat flux transferred to the biomass in the pyrolysis chambers. Ray effect due to the presence of baffles is studied and demonstrated to have a crucial effect on radiative heat flux on the walls of the pyrolysis rooms. Shadow effect caused by the presence of the baffles is also studied. The non grey radiative heat transfer is studied for the real existent configuration. The Weighted Sum of The Grey Gases (WSGG) Model of Kim and Song is used as non grey model. The effect of soot volumetric fraction on the non grey radiative heat flux is investigated and discussed.

Keywords—Baffles, Blocked-off region procedure, FVM, Heat recuperation, Radiative heat transfer, Shadow effect.

I. INTRODUCTION

OPTIMIZING the heat transfer in recuperation systems remains the essential care of heating engineers. However, the designs of heat recuperators have a crucial effect on the efficiency of energy conversion processes generally made at high temperature in complex geometries in presence of baffles. Numerical investigation of the number and position of

Mohamed Ammar Abbassi is with the Unité de Recherche Matériaux, Energie et Energies Renouvelables (MEER) Faculté des Sciences de Gafsa, B.P.19, Zarroug, Gafsa, 2112 (e-mail: MedAmmar.Abbassi@enim.rnu.tn).

Kamel Guedri is with the Mechanical Engineering Department, College of Engineering and Islamic Architecture, Umm Al-Qura University, KSA (e-mail: Kamel.Guedri@enim.rnu.tn).

Mohamed Naceur Borjini is with the University of Monastir, Rue Iben El Jazzar, 5019, Monastir, Tunisia (e-mail: naceur.borjini@fsm.rnu.tn).

Kamel Halouani is with the UR: Micro Electro Thermal Systems (METS-ENIS-IPEIS) Industrial Energy Systems Group, University of Sfax – Route Menzel Chaker B.P: 1172 – 3018, Sfax – Tunisia, (e-mail: kamel.halouani@ipeis.rnu.tn).

Belkacem Zeghmati is with the LAMPS, University of Perpignan, Via Domitia, 52 Avenue Paul Alduy, 66860Perpignan Cedex – France, (e-mail: zeghmati@univ-perp.fr).

these baffles leads to adjustment of heat recuperators and could have serious advantages for the design of new thermal conversion systems. Indeed, radiative heat transfer in geometries with segmented baffles has many engineering applications, e.g. boilers, furnaces, heat exchangers, internally cooled turbine blades, heated combustors and solar collectors. Enhancement techniques usually employ baffles attached to the heated surface so as to provide an additional heat transfer surface area. Many investigations have been focused on the baffle-walled enclosures. Most studies discussed the optimal baffle geometry that enhance heat transfer performance for a given pumping power or flow rate. Chang et al. [1] examined numerically a rectangular enclosure with two partitions with finite thickness centred at an adiabatic ceiling as well as floor, for which the working fluid was assumed to be a participating medium under a large temperature difference. While adopting the radial flux method as a radiation solving method, they worked on a numerical manipulation of radiatively opaque obstructions in a computational domain. However, due to the technique used therein, an additional radial grid had to be introduced for a radiation solver, which is totally different from the usual grid configuration used for solving a flow field. Borjini et al. [2] solved the radiative heat transfer problem in a three-dimensional partitioned rectangular enclosure containing absorbing-emitting and isotropic scattering medium in the presence of heat generation. The shadowing partition effect is discussed for different optical medium properties and partition surface emissivities. They showed that the effect of the partition is more important in the upper half of the furnace and near the exit-end wall. A strong absorbing emitting medium attenuates the partition effect. On the other hand, the gas transmits the effect of the presence of the obstacle to surfaces that are not influenced by the shadow effect in transparent media. The emissivity of the partition has a significant effect on both radiative wall fluxes and gas temperature distributions. Han and Baek [3] studied numerically radiation-affected steady-laminar natural convection in a rectangular enclosure with two partitions. Pure convection, convection with surface radiation, and convection with surface/gas radiation are considered and compared. The effects of two incomplete partitions on thermofluid dynamics behavior are assumed to be very thin and adiabatic. It was found that the radiation played a significant role in developing the fluid dynamic and thermal distributions compared with cases

without radiation. The baffle configuration was also found to affect the results of radiation. Biomass inside the two pyrolysis rooms (Fig. 1) is heated and dried by the combustion of a quantity of biomass wastes in the combustor. The duration of this phase depends on the biomass initial moisture. At the beginning of the operating cycle of the biomass decomposition the released gases consists of CO, CO_2, some light hydrocarbons (methane-ethane-ethylene), formic acid, acetone, methanol, and light tar. Pyrolysis gases are premixed with the ambient air before introduced in the combustor. When the pyrolysis reactions produce a sufficient quantity of fuel gas to ensure the needed energy for biomass pyrolysis, the alimentation of the combustor by biomass wastes is stopped. The gases combustion energy is used to heat the biomass pyrolysis chambers through the heat recuperator before being rejected into the atmosphere via a chimney. More details of the operation cycle of the pilot plant are given in [4]-[6]. In the proposed biomass pyrolysis pilot plant (Fig. 1) [4]-[6] the radiant energy transport is an essential and very predominating phenomenon because the measured temperatures are very high (up to 1900K) [6]. The need for quantification of the radiative transfer leads to an increased request for developing radiation methods able to describe the physical reality. The considered heat recuperator (Fig. 2) has a complex shaped geometry, so analytical or exact solutions are unable to model radiation transfers inside the recuperator. Therefore, the choice of a resolution model should give the physical reality of the studied system with a reasonable computing time. The Finite Volume Method introduced by Raithby and Chui [7] offers a good compromise between accuracy and computing time and can be easily incorporated in computational fluid mechanics codes which involve radiating gases at high temperatures.

1. Chimney
2. Pyrolysis chambers
3. Pyrolysis gases channels
4. Heat recuperator
5. Pyrolysis gases combustor
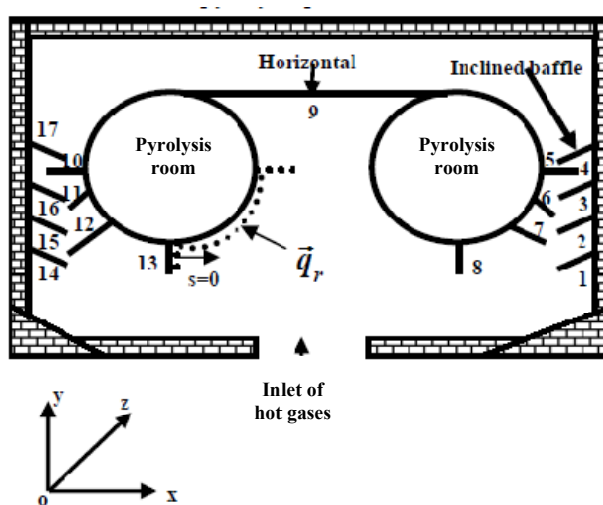6. Air combustor inlet

Fig. 1 Pilot plant

Fig. 2 Geometrical characteristics of the heat recuperator

The characterization of an infra-red active gas mixture results in the evaluation of the spectral radiative properties. The various models presented in the literature [8], [9] lead to various degrees of accuracy but the most accurate remains the line-by-line (LBL) model. The choice of a resolution model depends on the considered application as well as the degree of accuracy to be achieved. The WSGG model was initially developed by Hottel and Sarofim [10] in the context of the zonal method. It consists in simulating the total radiative properties of a gas mixture present in the thermal processes at high temperatures. Modest [11] showed that the WSGG model can be applied to any solution method of the RTE. Soufiani et al. [12] established a comparison between the results of the WSGG model and those obtained by the SNB model. The authors have found that the absorption by cold gases of radiation emanating from hot walls or gases is generally underestimated by the WSGG model. To resolve this problem Modest [13] proposed a solution which consists in using a total absorptivity depending on the whole temperature and concentration ranges along a path length. On the other hand, Young et al. [14] studied theoretically the relation between weighting factors used in the WSGG model for a mixture of non-grey gas and scattering grey particles in the thermal non-equilibrium, they numerically showed that a gas concentration variation yields a noticeable change in the radiative heat transfer when suspended particle temperature was different from the gas temperature. Kim and Song [15] developed the WSGG model based on the absorption coefficient as a function of pressure, temperature and model parameters. They found that the proposed model is accurate and versatile either in total or spectral calculations. Coelho [16] presented 3D numerical solutions of radiative heat transfer from non-grey gases by the DOM and DTM. Several gas radiative properties model namely the correlated k-distribution (CK), the spectral line-based weighted-sum-of-grey-gases (SLW) and the weighted-sum-of-grey-gases (WSGG) model are used. This study demonstrated that the WSGG model is computationally economical and has moderate accuracy. Abbassi et al. [17] presented a radiative heat transfer solutions for an industrial combustor of wood carbonization fumes using the FVM in conjunction with the WSGG model. A uniform mixture of CO_2 and H_2O vapor is considered. The effects of soot volumetric fraction, partial pressure ratio, and particle concentration on the inner wall radiative heat flux of the combustor are presented. The main objective of the present work is to determine which configuration of the baffles is better to enhance heat transfer to the two pyrolysis rooms (Fig. 2). The FVM is applied in conjunction with the blocked-off-region procedure and the WSGG model to study radiative exchanges in the heat recuperator containing CO_2/H_2O mixtures and soot particles. We will present firstly the results for a grey medium without scattering and then those for non grey mediums with anisotropic scattering. The effect of soot volume fraction on the inner wall radiative heat flux is also investigated.

II. MATHEMATICAL MODEL

A. Radiative T Transfer Equation

The radiative heat transfer in the heat recuperator containing a mixture of gas, soot, and particles is governed by the following equation:

$$\frac{dI_\eta}{ds} = -\left(\kappa_{g,\eta} + \kappa_{p,\eta} + \kappa_{s,\eta} + \sigma_{sp,\eta} + \sigma_{ss,\eta}\right)I_\eta + \kappa_{g,\eta}I_{b,g\eta} + \kappa_{p,\eta}I_{b,p\eta} + \kappa_{s,\eta}I_{b,s\eta} \quad (1)$$
$$+ \frac{(\sigma_{sp,\eta} + \sigma_{ss,\eta})}{4\pi}\int_{4\pi}\Phi_\eta(\vec{s},\vec{s}')I_\eta(\vec{s}')d\Omega'$$

where $\kappa_{g,\eta}$, $\kappa_{p,\eta}$ and $\kappa_{s,\eta}$ are respectively the spectral absorption coefficients of gas, particles and soot at the specific wave number η. $\sigma_{sp,\eta}$ and $\sigma_{ss,\eta}$ are the spectral scattering coefficients of particles and soot at the specific wave number η, respectively.

B. Boundary Conditions

When using the WSGG model to study the non-grey gas behaviour, bounding walls are assumed to be grey and diffusely emitting and reflecting radiation. Under these assumptions, the radiation intensity at a given boundary node is discretized as:

$$I_k(s_w,\mathbf{\Omega}) = \varepsilon_w w_k I_{b,k}(s_w) + \frac{1-\varepsilon_w}{\pi}\int_{\mathbf{\Omega'}.\mathbf{n_w}<0}I_k(s_w,\mathbf{\Omega'})\left|\mathbf{\Omega'}.\mathbf{n_w}\right|d\Omega' \quad (2)$$

In order to simplify the problem, the following assumptions are used:

- Temperature distribution in the heat recuperator is constant and uniform (soot, particles).
- The soot is assumed to be produced uniformly in all regions of the heat recuperator.
- Heat generation rate in each control volume is constant and uniform.
- The refractive index in each control volume is constant and uniform.

C. Discretization of the RTE

Assuming that the mixture contains non-grey gases, grey particles and grey soot particles the radiative transfer equation integrated over the kth grey band is written as:

$$\begin{cases} \frac{dI_k}{ds} = -(\kappa_{g,k} + \kappa_p + \kappa_s + \sigma_{sp} + \sigma_{ss})I_k + \kappa_{g,k}w_{g,k}I_{b,g} + \kappa_p w_{p,k}I_{b,p} + \kappa_s w_{s,k}I_{b,s} + S_k \quad (3) \\ S_k = \int_{\eta_-^k}^{\eta_+^k}\left[\frac{(\sigma_{sp,\eta} + \sigma_{ss,\eta})}{4\pi}\int_{4\pi}\overline{\Phi}_\eta^{l'l}I_\eta(\vec{s}')d\Omega'\right]d\eta \end{cases}$$

where $\overline{\Phi}^{l'l}$ is the average scattering phase function. The simultaneous spatial and angular discretizations of (3) lead to:

$$\sum_{i=w,e,s,n}(I_{ki}^l\Delta A_i N_i^l) = \begin{cases} -(\kappa_{g,k} + \kappa_p + \kappa_s + \sigma_{sp} + \sigma_{ss})I_k + w_{g,k}(T)\kappa_{g,k}I_{b,g} \\ + w_{s,k}(T)\kappa_s I_{b,s} + w_{p,k}(T)\kappa_p I_{b,p} + S_k \end{cases} \quad (4)$$

Young et al. [14] demonstrated that if the gas, particles and soot particles share the same K^{th} grey band and are at thermal non-equilibrium, we obtain $w_{p,k} = w_{g,k}(T)$ and $w_{s,k} = w_{g,k}(T)$. Under these assumptions and developing the first term of (4), the latter equation becomes:

$$(I_{ke}^l - I_{kw}^l)\Delta y N_{cx}^l + (I_{kn}^l - I_{ks}^l)\Delta x N_{cy}^l =$$

$$\begin{bmatrix} -(\kappa_{g,k} + \kappa_p + \kappa_s + \sigma_{sp} + \sigma_{ss})I_{kp} \\ + w_{g,k}(T)\kappa_{g,k}I_{bp,g} + w_{g,k}(T)\kappa_s I_{bp,s} \\ + w_{g,k}(T)\kappa_p I_{bp,p} + S_k \end{bmatrix} \Delta x \Delta y \quad (5)$$

Equation (5) represents the conservation of radiant energy related to the Kth spectral band, within a control volume and for an elementary solid angle $\Delta\Omega^l$ centered on nodal point P.

D. The Blocked-off-Region Procedure

The blocked-off-region procedure consists on adding fictitious domains to the real physical domains in order to obtain a simple configuration where the solution of the RTE is easy to generate. The fictitious domains are regarded as areas physically inactive; therefore, the boundary conditions for the real domain are regarded as the solutions sought in the fictitious domains. To distinguish real domains from fictitious ones, an additional source term is added as:

$$S = S_C + S_p I_p^l \quad (6)$$

For a given real black boundary, the additional source term is chosen as follows: $(S_C, S_P) = (0,0)$ for the real domains and $(MI_b, -M)$ for the fictitious domains (M is a large number). Curved and inclined geometries can also be treated using this procedure but it needs a finer grid. To examine the effects of the baffles on radiative heat transfer calculations they are assumed to be very thin and adiabatic.

E. Radiative Properties of Gases

The weighted sum of the grey gases (WSGG) model consists of the division of the spectrum in m regions where the absorption coefficient is assumed constant. It assigns to a non-grey gas an equivalent finite number of grey gases with appropriate weighting factors strongly dependant on the local temperature. As the model of Kim and Song [15] is concerned, the absorption coefficient is regarded as a function of pressure, temperature and model parameters for water vapour, carbon dioxide and their mixtures as the following equation shows:

$$\kappa_{ai} = \kappa_{ai\circ} \frac{P_{abs}}{T^2} e^{-\frac{\alpha_i}{T}} \quad (7)$$

where $\kappa_{ai\circ}$ and α_i are model parameters for specie i. P_{abs} and T are the medium pressure and temperature respectively.

When the classical WSGG model is used for the solution of the non grey radiative transfer equation the absorption coefficient is written as: $\kappa_a = -Ln(1 - \varepsilon(L))/L$. To compute the local absorption coefficient within each control volume, some authors take the path length L as the mean beam length for the whole enclosure and for others it's considered as the mean effective path of that control volume. The present WSGG-based spectral model of Kim and Song calculates the absorption coefficient independently of L. This model will be used throughout this paper.

F. Radiative Properties of Particles

The particle absorption and scattering coefficients are defined respectively by:

$$\kappa_p = \varepsilon_p \sum_i N_i \frac{\pi d_i^2}{4} \quad (8)$$

$$\sigma_{sp} = (1 - \varepsilon_p) \sum_i N_i \frac{\pi d_i^2}{4} \quad (9)$$

The particle emissivity ε_p, the particle diameter and the particle density ρ are taken the same as in the work of Young et al. [14]. In (8) and (9), N_i and $(\pi d_i^2 / 4)$ are the particle number density and the particle projected area pertaining to group i, respectively.

The soot absorption coefficient used in the present work is taken in the Rayleigh scattering limit [17].

$$\kappa_s = \frac{3,72 f_v C_0 T}{C_2} \quad (10)$$

where $C_0 = 36 \pi n k / [(n^2 - k^2 + 2)^2 + 4n^2 k^2]$, $C_2 = 1,4388$ cm K, while $n=1,85$ is the real part of the complex index of refraction and, $k=0,22$ is the absorptive index. The soot scattering coefficient is given by the following equation:

$$\sigma_{ss,\eta} = \frac{4\alpha^4 f_v}{d} \frac{[(n^2 - k^2 - 1)(n^2 - k^2 + 2) + 4n^2 k^2]^2 + 36n^2 k^2}{[(n^2 - k^2 + 2)^2 + 4n^2 k^2]^2} \quad (11)$$

with $\alpha = \frac{\pi d}{\lambda}$ is the size parameter.

In the case of the present heat recuperator (medium with anisotropic diffusing particles) the scattering phase function for large particles is given by [18]:

$$\Phi(\theta) = \frac{8}{3\pi}(\sin\theta - \theta\cos\theta) \quad (12)$$

where θ is the angle between the incident and outgoing beams. When using the finite volume method for the

resolution of the radiative heat transfer equation with anisotropic scattering, the average scattering phase function $\overline{\Phi}^{l'l}$ is used in the final discretised equation. This average scattering phase function gives the average energy scattered from solid control angle defined by incident direction l' to solid control angle defined by direction l. It is calculated by the following expression:

$$\overline{\Phi}^{l'l} = \frac{\int_{\Delta\Omega^{l'}} \Phi(\vec{s}, \vec{s}') d\Omega'}{\Delta\Omega^{l'}} \qquad (13)$$

G. Radiative Heat Flux

The total intensity integrated over the entire spectrum is given by:

$$I = \sum_{\eta=1}^{M} I_\eta \Delta\eta \qquad (14)$$

where M is the number of total narrow-bands and $\Delta\eta$ is the narrow band width. The heat flux components are calculated as:

$$q_i = \int_{4\pi} \vec{n}_i . \vec{n}_0 I d\Omega = \sum_\eta \int_{4\pi} \vec{n}_i . \vec{n}_0 I_\eta \Delta\eta d\Omega \quad i=\text{x or y} \qquad (15)$$

where: $\vec{n}_i$ is the unit normal vector of a surface pointing to the gas side. $\vec{n}_0$ is the unit vector in the direction of radiation propagation.

The irradiation G or incident radiation is calculated by the following equation:

$$G = \int_{4\pi} I d\Omega \qquad (16)$$

III. VALIDATION OF THE NUMERICAL CODE

The validation of the numerical code for grey or non grey mediums is done in an earlier paper [17] and only for a non grey medium is reported here for the sake of brevity. The present computer code represents a developed version of the code employed in our previous study for non-grey media [17], [19]. The study of the non-grey case was carried out by the finite volume method (FVM) associated to the WSGG-based spectral model for a cavity, filled with water vapor, of length L and whose spacing is H with an infinite depth ($L=H=0.1m$). The lower and higher walls are supposed to be grey and isotropic diffusing with emissivity equal to ε =0.5. The other walls such as $x=0$ and L are regarded as black pseudo-walls, the medium is maintained at a unit total pressure, the concentrations of the species present are also supposed to be constant and the spectral range for H_2O varies from 150 to 4250 cm^{-1} as reported by Liu and Tiwari [20]. These authors used the Monte-Carlo technique and the statistical narrow-band (SNB) model taken here as a benchmark solution. For the WSGG-based spectral model, the considered spectrum is subdivided into 165 narrow-bands where each band contains 15 grey gases. The RTE is solved for each grey gas. Fig. 3 shows the radiative heat flux on the lower wall for three aspect ratios obtained with the WSGG-based spectral model compared with the results of Liu and Tiwari [20]. For the three aspect ratios, the results of the WSGG-based spectral model of Kim and Song [15] show little discrepancies with those of reference.
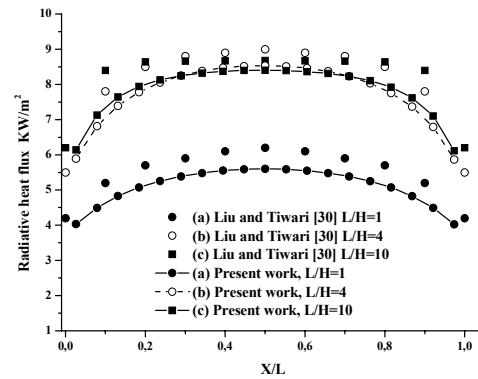

Fig. 3 Predicted profiles of radiative heat flux calculated by the WSGG model compared with the SNB benchmark data for test cases: (a) L/H=1, (b) L/H =4, (c) L/H =10

IV. RESULTS AND DISCUSSIONS

A. Heat Recuperator

The physical model of the studied heat recuperator is represented in Fig. 2. It consists of a parallelipepedic metallic construction containing two cylindrical chambers in direct contact with gases issued from biomass pyrolysis fumes combustion. To improve heat exchange and increase the residence time of hot gases ($T=1000-1500K$) in the heat recuperator, the metallic walls of the pyrolysis rooms, in direct contact with combustion gases, are equipped with several baffles. In fact, a horizontal baffle relates the two biomass pyrolysis rooms and inclined baffles are located on the walls of the pyrolysis rooms and the walls of the heat recuperator (Fig. 2). The external wall of the system is insulated by a thick layer of glass wool. The hot region is located at the bottom face of the recuperator, all other zones of the recuperator are supposed to be cold. The walls emissivities are taken equal to unity.

B. Computational Details

In order to test the reliability of the elaborated code for modelling radiative heat transfer in the recuperator many spatial and angular grids are used. In all calculations the step scheme is used. We have made the simulations with the following boundary conditions: hot face $T=1500K$, other faces $T=300K$, $\varepsilon = 1$ for all the faces, the extinction coefficient is taken as: $\beta = 0.2$, the scattering albedo is taken as: $\omega = 0$. The relative convergence criterion of the iterative procedure is

chosen as: $\left| \dfrac{I_p^n - I_p^{n+1}}{I_p^n} \right| < 10^{-4}$ where I_p^n is the intensity at

nodal point P and n is the iteration number. A cartesian uniform grid is used in all calculations. The cartesian equations of the two pyrolysis rooms and those of each baffle are determined and injected into the developed code in order to model them. The error between calculated temperatures and those of the reference case is calculated by the following equation:

$$e = \left(\frac{1}{N} \sum_i^N \frac{|T_{cal} - T_{ref}|}{T_{ref}} \right) \times 100 \qquad (17)$$

where T_{cal} is the calculated temperature and T_{ref} is the reference temperature (calculated from the 3D code supposed here as a benchmark solution [21]).

C. Grid Independence Study

In this paragraph the heat recuperator is supposed to contain a grey semi transparent medium. The number of spatial control volumes used for this calculation is varied as $(N_x \times N_y) = (46 \times 44)$, $(N_x \times N_y) = (62 \times 58)$,

$(N_x \times N_y) = (92 \times 86)$ and $(N_x \times N_y) = (184 \times 172)$ for a fixed number of angular control volumes equal to $(N_\theta \times N_\varphi) = (4 \times 24)$. Fig. 4 gives the effect of the spatial grid on the temperature profiles in the mid-plane of the recuperator versus the y direction. We obtained a grid independent solution for a spatial grid equal to $(N_x \times N_y) = (92 \times 86)$. This choice seems to be the best one in time computing (115.5 s), precision (error=10.7%), memory storage, and giving the real shape of the heat recuperator. Whereas a twice spatial grid $(N_x \times N_y) = (184 \times 172)$ needs 950.6 s but doesn't contribute to ameliorate the precision of the solution (error=10%) compared with 3D results (Fig. 4) using $(N_x \times N_y \times N_z) = (92 \times 86 \times 11)$ spatial grid and $(N_\theta \times N_\varphi) = (4 \times 24)$ angular grid. Consequently a spatial grid equal to $(N_x \times N_y) = (92 \times 86)$ will be retained in all the calculations throughout this paper.

The number of angular control angles used for this calculation is varied from $(N_\theta \times N_\varphi) = (4 \times 12)$, $(N_\theta \times N_\varphi) = (4 \times 24)$, $(N_\theta \times N_\varphi) = (4 \times 36)$ and $(N_\theta \times N_\varphi) = (4 \times 48)$ for a fixed number of spatial control volumes equal to $(N_x \times N_y) = (92 \times 86)$. Fig. 5 gives the effect of the angular grid on the radiative heat flux on the walls of the pyrolysis rooms versus the y direction. When varying the angular grid an oscillatory solution is found. The angular grid effect on solution accuracy is more important than the spatial grid effect. We obtained a grid independent solution for an angular grid equal to $(N_\theta \times N_\varphi) = (4 \times 24)$ with a CPU time

equal to 115.5s. This angular grid will be retained for all the calculations throughout this paper. Compared to the discrete ordinates method this angular grid corresponds to the S6 which are symmetric quadratures.
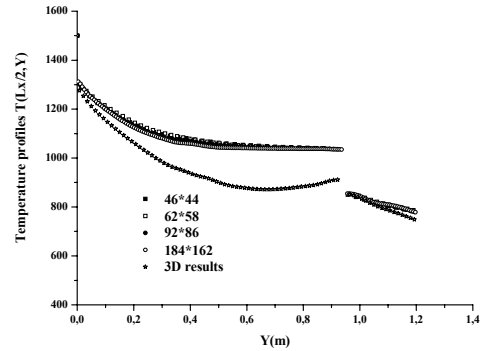

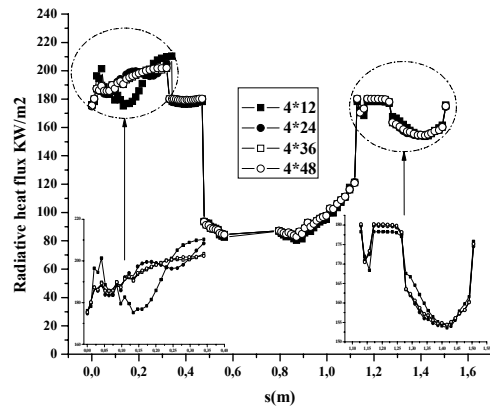Fig. 4 Comparison of temperature 2D results with 3D results

Fig. 5 Ray effect on radiative heat flux on the walls of the pyrolysis rooms for the different considered cases

D. Effect of the Baffles Configuration

In this study we suppose that the depth of the heat recuperator is greater than the other dimensions so that the transfers can be described by a two-dimensional model. Also we made a comparison study between 2D and 3D results for the temperature pattern as given in Fig. 6 results are in good agreement and the discrepancies are about 10%. The 3D results are those of the code used in our recent work [21]. In order to determine the best configuration of the baffles eight cases are studied (Fig. 6). In each case we tried to add baffles and studied its effect on temperature distribution inside the heat recuperator and radiative heat flux on the walls of the pyrolysis rooms. The main objective of our study is to peak out the case giving the greatest radiative heat flux transferred to the two pyrolysis rooms. This heat will be the energy source for biomass pyrolysis.

Case 1. The heat recuperator consists of only two pyrolysis rooms (Fig. 6 (a)).

Case 2. Compared to Case 1, we add one horizontal baffle which relates the two pyrolysis rooms. (Fig. 6 (b), Baffle 9).

Case 3. We add to Case 2 four inclined baffles on the right wall and four inclined baffles on the left wall. (Fig. 6 (c), Baffles number 1,2,3,4,14,15,16, and 17).

Case 4. We add to Case 3 one vertical baffle on pyrolysis room 1 and one vertical baffle on pyrolysis room 2. (Fig. 6 (d). baffles number 8, 13).

Case 5. We eliminate baffles number (1,2,3,4,14,15,16, and 17) from Case 4 and added three inclined baffles on pyrolysis room 1 (Baffles 5,6, and 7) and three inclined baffles on pyrolysis room 2 (Baffles 10, 11, and 12). (Fig. 6 (e)).

Case 6. To case 5 we added four inclined baffles on the right wall (Fig. 6 (f). Baffles 1,2,3, and 4) and four inclined baffles on the left wall (Fig. 6 (f). Baffles 14,15,16, and 17), this case represents the real recuperator given in Fig. 2.

Case 7. Compared with the case 6 we displaced the location of baffles 8 and 13 as given by Fig. 6 (g).

Case 8. Compared with case 6 we removed the baffles number 8 and 13 as given by Fig. 6 (h).

Case 1 (a)   **Case 2 (b)**

Case 3 (c)   **Case 4 (d)**

Case 5 (e)   **Case 6 (f)**

Case 7 (g)   **Case 8 (h)**
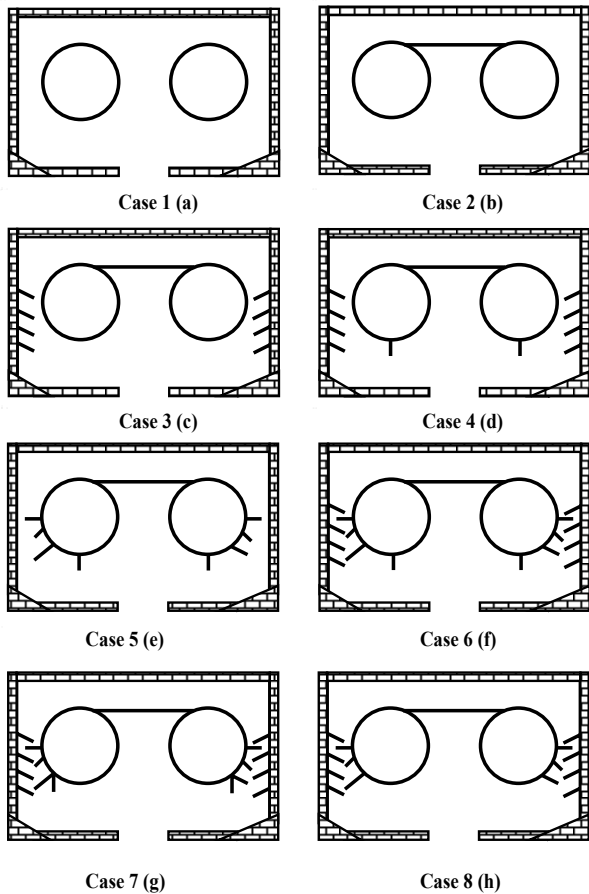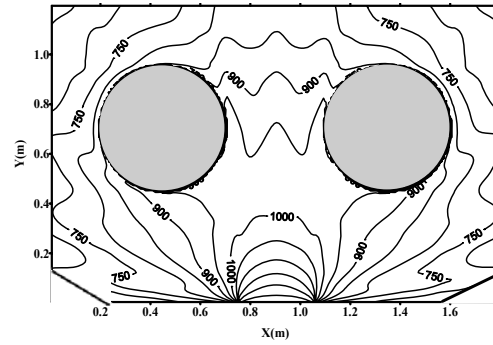
Fig. 6 Different studied configurations

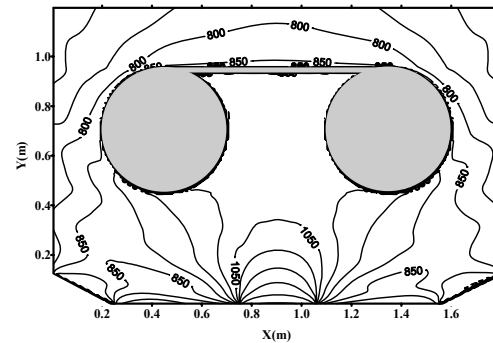Fig. 7 (a) Temperature distribution for Case 1 (K)

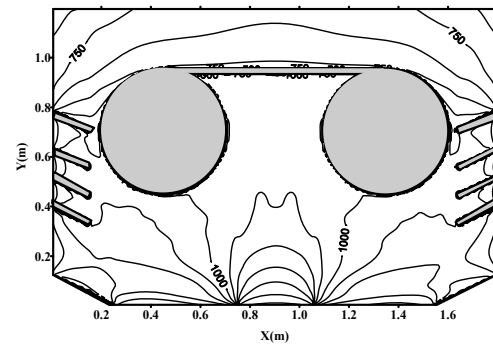Fig. 7 (b) Temperature distribution for Case 2 (K)

Fig. 7 (c) Temperature distribution for Case 3 (K)
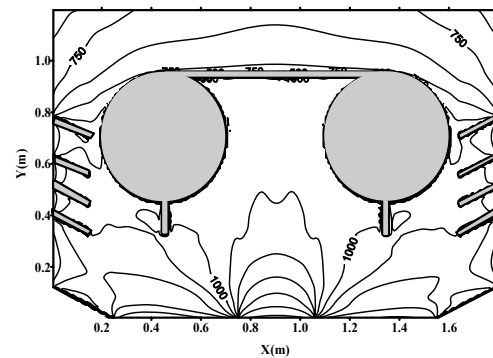

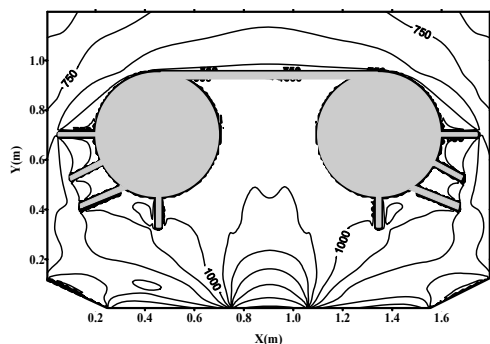Fig. 7 (d) Temperature distribution for Case 4 (K)

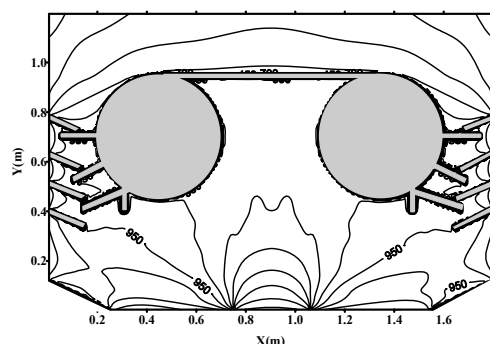Fig. 7 (e) Temperature distribution for Case 5 (K)

Fig. 7 (f) Temperature distribution for Case 6 (K)
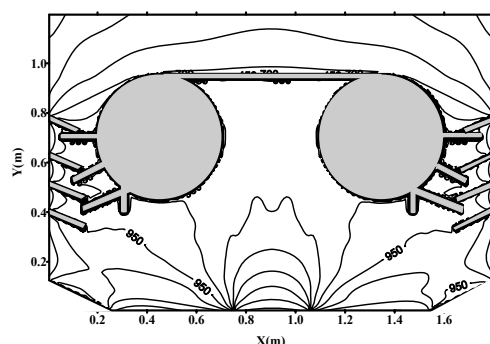

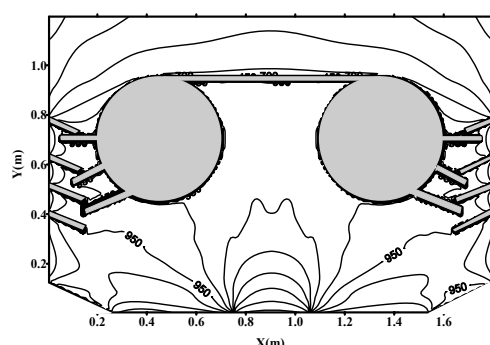Fig. 7 (g) Temperature distribution for Case 7 (K)

Fig. 7 (h) Temperature distribution for Case 8 (K)

Fig. 7 gives the temperature field inside the heat recuperator for the eight studied cases. For all cases we can see that the radiant energy is directed from the hot regions towards the cold zones. We notice that the radiative heat flux increases near the hot region and decreases in proximity of the cold faces. The calculated radiative heat flux (q_r) at the pyrolysis rooms is as shown by the dotted lines (Fig. 2). In these calculations we assumed that the divergence of the radiative heat flux is null ($\nabla . \vec{q}_r = 0$).

Fig. 7 (a) gives temperature distribution inside the heat recuperator for case 1. The mean temperature calculated is equal to 739.88 K and the mean radiative heat flux on the walls of the pyrolysis rooms is equal to 124.21 kW/m^2.

Fig. 7 (b) gives temperature pattern inside the heat recuperator for case 2. For this case the added horizontal baffle contributes to the increase of the mean medium temperature, which is equal to 767.7 K. This demonstrates that this baffle has an important role to slow down gases and keeping radiant energy located between the two pyrolysis rooms. The mean radiative heat flux on the walls of the pyrolysis rooms is equal to 139.06 kW/m^2. For this case we can see clearly that near the horizontal baffle which links the two pyrolysis rooms the temperature increases. We notice the appearance of a stagnation zone where the temperature is equal to 1000K; the area of this stagnation zone increases when increasing the number of baffles.

Fig. 7 (c) shows temperature pattern for case 3. The calculated mean medium temperature is equal to 790.27 K and the mean radiative heat flux on the walls of the pyrolysis rooms is equal to 148.44 kW/m^2. We noticed that adding these baffles increases the radiative heat flux transferred to the pyrolysis rooms. (9 kW/m^2) and significantly increases the mean medium temperature (23 K).

Fig. 7 (d) shows temperature distribution inside the heat recuperator for case 4. The calculated mean temperature is equal to 790.45 K and the mean radiative heat flux is equal to 147.43 kW/m^2. We noticed that for this case the mean temperature is the same as the case 3, whereas the mean radiative heat flux is decreased. Therefore adding baffles number 8 and 13 on the walls of the pyrolysis rooms contributes to the augmentation of the radiative heat flux but doesn't have a sensible effect on temperature distribution. This is due to the augmentation of the exchange area between the pyrolysis rooms and the combustion medium. This result shows also that the baffles slow down the hot fumes which participate to heat the pyrolysis rooms.

Fig. 7 (e) gives temperature pattern inside the heat recuperator versus x and y directions for case 5. For this case the mean temperature is shown to increase and is equal to 778.62 K and the radiative heat flux is slightly decreased and is equal to146.58 kW/m^2.

Fig. 7 (f) gives the temperature pattern in the real configuration of the heat recuperator with all baffles as shown by Fig. 2. The calculated mean temperature is equal to 786.22K and the mean radiative heat flux is equal to 149.74KW/m^2. We concluded that the existent real configuration of the heat recuperator isn't the best one when considering only radiative heat transfer.

Fig. 7 (g) gives the temperature pattern in the heat recuperator where we displaced baffles number 8 and 13 as shown by Fig. 6 (g). The calculated mean temperature is equal to 785.82 K and the mean radiative heat flux is equal to 151.04 kW/m^2; we noticed that for this case the mean radiative heat flux is the greatest one.

Fig. 7 (h) gives the temperature pattern in the heat recuperator where we removed baffles number 8 and 13. The calculated mean temperature is equal to 787.25 K and the mean radiative heat flux is equal to 150.73 kW/m^2. It springs from this study that the configuration of the heat recuperator given by Fig. 6 (g) is the best one allowing the maximum radiative heat transferred to biomass inside the two pyrolysis rooms. Also the radiative heat flux on the walls of the pyrolysis rooms increases as the number of baffles put on the pyrolysis rooms is increased as shown by Fig. 8. The location of the baffles has a very important effect on radiative heat transfer. The heat recuperator temperature increases when increasing the baffles number as given by Fig. 9 because the baffles stopped the hot gases which will give more heat to the medium before rejected into the atmosphere. We concluded that when baffles are put on the walls of the two pyrolysis rooms they will increase the exchange area and consequently more radiative energy is transferred to biomass inside the two pyrolysis rooms. Whereas, if baffles are put on the walls of the heat recuperator (Baffles number 1, 2, 3, 4, 14, 15, 16, and 17) they will enhance the loss of radiative energy to the ambient medium then the efficiency of the heat recuperator decreases.

Shadow effect is defined as an area that is not or is only partially irradiated or illuminated because of the interception of radiation by an opaque object between the area and the source of radiation. In the framework of radiation between surfaces shadow effect due to surface irregularities is essential in computing radiative intensities. In order to estimate this effect, one needs to find a part of the surface that is simultaneously both illuminated by the light source and visible to the observer [22]. In order to investigate the shadow-hiding effect, computer simulations are carried out inside the heat recuperator for different number of baffles to examine effects of the baffle on heat transfer distributions. First the heat recuperator contains only the two pyrolysis rooms, then one add the baffles in order to study their effect on the internal radiative heat flux and on temperature distribution. Based on the calculations we showed that as the number of baffles put on the pyrolysis rooms increases, the medium temperature increases and the radiative heat flux on the walls of the pyrolysis rooms increases. In fact, the maximum temperature versus the cases number is shown in Fig. 8. It is interesting to note that the baffles number (8 and 13) must be chosen as given by Fig. 6 (g) because this situation diminishes the shadow effect therefore more radiative heat is transferred to the pyrolysis chambers containing biomass to be pyrolysed. If the baffles are located on the pyrolysis rooms near the inlet (hot wall), as given by Fig. 6 (f), the radiative heat flux increases whereas if one puts the baffles on the pyrolysis rooms near the cold wall the radiative heat flux transferred to the pyrolysis rooms decreases. In a pure radiation problem the

baffles which are located on the external walls of the recuperator contribute to increase the radiative heat flux transferred to the pyrolysis rooms. Increasing the number of these baffles increases the amount of radiative heat flux transferred to the pyrolysis rooms. In a combined radiation-conduction problem the baffles located on the walls of the pyrolysis rooms will enhance the heat flux transferred to biomass by conduction and by radiation. Whereas, the baffles located on the external walls of the recuperator will enhance the loose of heat flux by conduction and radiation because the temperature of the recuperator external walls is cold compared to the inlet gases temperature which is hot.
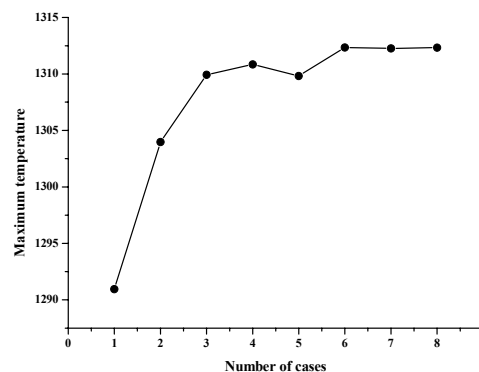

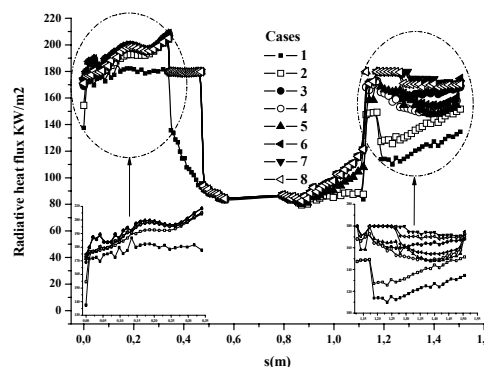Fig. 8 Maximum temperature versus the cases number, K

Fig. 9 Radiative heat flux on the walls of the pyrolysis rooms for the different considered cases

E. Influence of Soot Volume Fraction

In this study the heat recuperator medium is supposed to be non grey and containing soot particles. The heat recuperator contains *17* baffles inclined or vertical and put on the external walls of the heat recuperator or on the walls of the pyrolysis rooms (Fig. 2). Each baffle has a finite width. The conditions of all boundaries, including the surfaces of the baffles, were taken as *300K* in temperature, except at the inlet where the temperature was taken as *1500K* and a black body surface was assumed. The pyrolysis gases combustion products are composed of carbon dioxide (CO_2) and water vapour (H_2O) at atmospheric pressure. The mole fractions of CO_2 and H_2O are assumed to be uniform at *1/3* and *2/3*, respectively. The spectral range under consideration lies from *150* to *6000 cm^{-1}*

and each band, divided into *30* grey gases, has a spectral resolution of *25cm^{-1}*. The combustion gas is assumed to be homogeneous all over the heat recuperator. All the interior walls delimiting the medium are supposed to be grey and isotropic diffusing in emission as in reflexion. The soot volume fraction is supposed to be uniform in all regions of the heat recuperator. The medium is divided into *92× 86* uniform finite control volumes and an angular mesh *4× 24* finite control angles. The heat recuperator inner walls are grey diffusing and emitting the radiative energy, with emissivities equal to *0.8*.

In order to analyze the effect of soot volume fraction on the wall radiative heat flux of the pyrolysis rooms, we assume that the medium contains only a mixture of gas (H_2O and CO_2) and soot; all other properties of the medium are kept unchanged. Three values of soot volume fraction are considered in the present work ($f_v=10^{-7}$, 10^{-6}, and 10^{-5}). The distribution of wall heat flux as function of soot volume fraction is illustrated in Fig. 10. It is found that when the soot volume fraction increases the value of the wall heat flux is shown to increase. This can be explained by the fact that when the soot volume fraction increases the medium thermal inertia becomes more important and soot emits a fraction of the radiative energy which is absorbed by the pyrolysis room's wall.

V. CONCLUSION

Results from numerical simulations of two-dimensional grey/non grey heat radiation in a geometrically complex heat recuperator are used to examine effects of baffles on radiative heat transfer. The finite volume method (FVM) is used to solve the radiative heat transfer equation. The blocked-off region procedure is applied to treat the geometrical irregularities. The weighted sum of the grey gases (WSGG) model of Kim and Song is used as a non grey gas model. The effect of the baffles location on radiative heat flux is investigated and demonstrated to be advantageous. Shadow effect is studied and demonstrated to have a crucial effect on wall radiative heat flux. Also, if the baffles are located on the walls of the pyrolysis rooms near the inlet (hot regions) they will contribute to enhance the heat transfer to biomass. Whereas, if the baffles are located near the outlet or on the external walls of the heat recuperator (cold regions) they will contribute to the loss of radiative energy. It springs from this study that the soot volume fraction affects strongly the radiation heat flux within the combustors of biomass pyrolysis smokes. Finally, this work can be improved by studying the non-homogenous behaviour of the heat recuperator medium or studying combined conduction and radiation in order to evaluate heat losses by conduction within the recuperator walls.
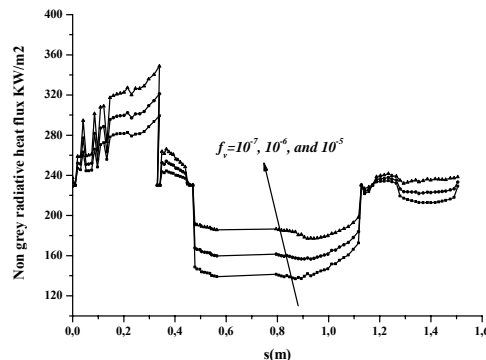

Fig. 10 Effect of soot volume fraction on radiative heat flux on the walls of the pyrolysis rooms

TABLE I
AVERAGE CALCULATED RADIATIVE HEAT FLUX AND TEMPERATURES FOR THE DIFFERENT STUDIED CASES

Case	1	2	3	4	5	6	7	8
T_m	740	768	790	790	779	786	786	787
Q_m	124	139	148	147	147	150	151	151

REFERENCES

[1] L. C. Chang, K. T. Yang, and J. R. Lloyd, Radiation-natural convection interactions in two-dimensional complex enclosures, Journal of Heat Transfer, Vol. 105, pp. 89-95, 1983.

[2] M. N. Borjini, H. Farhat and M.-S Radhouani, Analysis of radiative heat transfer in a partitioned idealized furnace, Numerical Heat Transfer, Part A, Vol. 44, pp. 199-218 , 2003.

[3] C. Y. Han and S. W. Baek, The effects of radiation on natural convection in a rectangular enclosure divided by two partitions, Numerical Heat Transfer, Part A: Applications, Vol.37, No.3, pp. 249-270, 2000.

[4] M.A. Abbassi, K. Halouani, X. Chesneau, B. Zeghmati and A. Zoulalian, Modélisation des transferts thermiques couplés à la cinétique réactionnelle dans une chambre de combustion des gaz de pyrolyse de la biomasse, Congrès Français de Thermique, Toulouse, 3-6 juin, pp. 765-770, 2008.

[5] M.A. Abbassi, N. Grioui, K Halouani, A. Zoulalian and B. Zeghmati, Racing modeling of the combustion in a pilot furnace of fumes produced from wood carbonization, ASME ATI, Conference, Milan Italy, 14-17 may, pp. 61-69, 2006.

[6] M.A. Abbassi, N. Grioui, K Halouani, A. Zoulalian and B. Zeghmati, A practical approach for modelling and control of biomass pyrolysis pilot plant with heat recovery from combustion of pyrolysis products, Fuel Processing Technology, Vol. 90, pp. 1278-1285, 2009.

[7] G.B. Raithby and E.H. Chui, A finite volume method for predicting a radiant heat transfer in enclosures with participating media, J. Heat Transfer Vol. 112, pp. 415-423, 1990.

[8] J. Taine and A. Soufiani, From spectroscopic data to approximate models, Adv. Heat transfer Vol.33 pp. 295-414, 1999.

[9] V. Goutiere, F. Liu , A. Charette, An assesement of real-gas modelling in 2D enclosures, J. Quant. Spectroscopic. Radiat. Transfer, Vol. 64, no. 3, pp. 299-326, 2000.

[10] H. C Hottel and A.F Sarofim., Radiative transfer, New York, 1967.

[11] M. F. Modest, The weighted-sum-of-gray-gases model for arbitrary solution methods in radiative transfer. ASME J. of Heat transfer, Vol.113, pp. 650-656, 1991.

[12] A. Soufiani and E. Djavdan, A Comparison between weighted sum of gray gases and statistical narrow-band radiation models for combustion applications, Combustion and Flame, Vol. 97, pp. 240-250, 1994.

[13] M. F. Modest, Radiative Heat Transfer, Mc Graw-Hill, 1993.

[14] M. Young, Yu, S.W. Baek and J. H. Park, An extension of the weighted sum of the gray gases non-gray gas radiation model to a two phase mixture of non-gray gas with particles, Int. J. Heat Mass Transfer, Vol. 43, pp. 1699-1713, 2000.

[15] O.J. Kim and T.H Song, Data base of WSGGM-based spectral model for radiation properties of combustion products, J. Quant. Spectrosc. Radiat. Transfer, Vol. 64, pp. 379–394, 2000.

[16] P. J. Coelho, Numerical simulation of radiative heat transfer from non-gray gases in three-dimensional enclosures, J. Quant. Spectroscopic. Radiat. Transfer, Vol. 74, pp. 307-328, 2002.

[17] M.A. Abbassi, K.Halouani, M.S. Radhouani, and H. Farhat, A parametric study of radiative heat transfer in an industrial combustor of wood carbonization fumes. Numerical Heat Transfer, Part A : Vol. 47, pp. 825-847, 2005.

[18] C.L. Tien, Thermal radiation in packed and fluidized beds, Journal of Heat Transfer, Vol. 110, pp.1230-1242, 1988.

[19] K. Guedri, M.N. Borjini, R. Mechi, and R. Said, Formulation and testing of the FTn finite volume method for radiation in 3-D complex inhomogeneous participating media, J. Quant. Spectrosc. Radiat. Transfer, Vol. 98, pp. 425-445, 2006.

[20] F. Liu and S. N. Tiwari, Investigation of two-dimensional radiating using a narrow band model and Monte Carlo Method, in radiative heat transfer: theory and applications, ASME HTD-Vol. 244, pp. 21-31, 1993.

[21] K. Guedri, M.A. Abbassi, M. N. Borjini and K. Halouani, Application of the finite-volume method to study the effects of baffles on radiative heat transfer in complex enclosures, Numerical Heat Transfer, Part A : Vol. 55, pp. 1-27, 2009.

[22] D.G. Stankevich, Y.G. Shkuratov, K. Muinonen, Shadow-hiding effect in inhomogeneous layered particulate media, J. Quant. Spectrosc. Radiat. Transfer, Vol. 63, pp. 445-458, 1999.